frontiers | Frontiers in Earth Science

TYPE Original Research
PUBLISHED 17 July 2024
DOI 10.3389/feart.2024.1407967

OPEN ACCESS

EDITED BY
Yongqiang Chen,
Commonwealth Scientific and Industrial Research Organisation (CSIRO), Australia

REVIEWED BY
Zhongxiang Zhao,
Yangtze University, China
Ran Zhang,
Sinopec, China
Qing He,
University of Alberta, Canada

*CORRESPONDENCE
Kun Tian,
973353569@qq.com

RECEIVED 27 March 2024
ACCEPTED 13 June 2024
PUBLISHED 17 July 2024

CITATION
Tian K, Qiao X, Zhou J, Xue C, Cao J, Yin X, Lv S and Zhugeng B (2024), Pore structure characteristics and influencing factors of dolomite reservoirs: a case study of the lower Ordovician Majiagou Formation, Ordos Basin, China.
Front. Earth Sci. 12:1407967.
doi: 10.3389/feart.2024.1407967

Pore structure characteristics and influencing factors of dolomite reservoirs: a case study of the lower Ordovician Majiagou Formation, Ordos Basin, China

Kun Tian[1]*, Xiangyang Qiao[1], Jinsong Zhou[1], Chunqi Xue[2], Jun Cao[1], Xiao Yin[1], Shuo Lv[3] and Bolun Zhugeng[1]

[1]Natural Gas Research Institute of Shaanxi Yanchang Petroleum Group Co., Ltd., Xi'an, China, [2]Oil and Gas Technology Research Institute, PetroChina Changqing Oilfield Company, Xi'an, Shaanxi, China, [3]Research Institute of Shaanxi Yanchang Petroleum Group Co., Ltd., Xi'an, China

The evaluation of the pore structure in dolomite, particularly with regard to pore heterogeneity, geometry, and connectivity, is crucial for oil and gas field production and reservoir prediction. The subsalt dolomite reservoir in the Ordovician strata of the Ordos Basin has shown promising exploration results and is anticipated to have a high hydrocarbon potential. However, there has been limited research on the pore structure and primary controlling factors of the Ordovician Majiagou reservoir in the south-central Ordos Basin. Therefore, we conducted a comprehensive analysis of the pore structure and fractal characteristics using routine petrophysical measurements, thin-section analysis, and high-pressure mercury injection (HPMI) data. We also discussed the relationship between fractal dimension, reservoir physical properties, and pore structure, along with exploring the origin of potentially prolific reservoirs. Our observations from the thin section identified four main pore types: intercrystalline pores, intercrystalline dissolved pores, dissolved pores, and micro-fractures. The data from HPMI revealed that the average pore–throat radii range from 0.009 μm to 0.015 μm with porosity ranging from 0.4% to 5.26%, and permeability ranging from 0.011 mD to 0.059 mD. They were further categorized into three reservoir types: dissolved pore type, intra-crystalline (dissolved) pore type, and micro-porous type. The fractal dimension was calculated based on HPMI data, and the reservoir's fractal characteristics were divided into two segments. The dissolved pore type was identified as the potentially prolific reservoir due to its larger pore size and volume, moderate permeability, and homogeneity on pore structure. Additionally, the fractal dimension is negatively correlated with porosity and permeability and positively correlated with sorting coefficient and skewness, suggesting that fractal dimensions are valuable for evaluating reservoir quality and quantitatively characterizing pore networks.

KEYWORDS

pore structure, fractal characteristics, high-pressure mercury injection, dolomite reservoir, Ordos Basin

1 Introduction

With the improvement of exploration and development technology, the carbonate rock associations are considered potentially significant contributors to the global crude oil supply (Luo et al., 2008; Ma et al., 2017; Yang et al., 2018). The oil and gas reserves in these types of rocks are widespread in China, including the Cambrian–Ordovician system in the Tarim Basin, the Paleozoic and Triassic system in the Sichuan Basin, and the Lower Ordovician series in the Ordos Basin, which have become an important part of increasing oil and gas storage and production (Lai et al., 2019; Zhao et al., 2012). However, carbonate reservoirs have strong heterogeneity and complex pore structure, making the exploitation and prediction of prolific reservoirs difficult.

Currently, researchers have utilized a variety of advanced methodologies such as petrographic observation, scanning electron microscopy (SEM), transmission electron microscopy (TEM), field emission scanning electron microscopy (FE-SEM), X-ray computed (micro) tomography, nuclear magnetic resonance (NMR), high-pressure mercury injection (HPMI), and incremental pressure mercury injection (IPMI) to characterize pore types, pore geometry, pore connectivity, pore size distribution, and pore volume on carbonate reservoirs (Gane et al., 2004; Sok et al., 2010; Jouini et al., 2011; Gundogar et al., 2016; Oyewole et al., 2016; Tan et al., 2020; Wang et al., 2020; Zhang et al., 2022). Additionally, they have investigated the relationship between carbonate reservoir and structure, sedimentation process, and rock mineral composition (Wei et al., 2017; Zhang et al., 2018). In recent years, several studies have proposed that high fractal dimension is associated with highly heterogeneous pore networks (Mastalerz et al., 2012; Melnichenko et al., 2012; Pan et al., 2016; Mendhe et al., 2017). Consequently, fractal dimensions can be employed to assess the pore heterogeneity of carbonate reservoirs to provide valuable insights into fluid flow properties and exploitation (Hulea and Nicholls, 2012; Menke et al., 2017).

However, limited research has been conducted on the heterogeneity characteristics of carbonate reservoirs in the Ordovician Majiagou Formation in the middle-southern region of the Ordos Basin. Therefore, this study aims to analyze the pore structure and fractal characteristics of carbonate reservoirs through cast thin-section analysis, routine petrophysical measurement, and HPMI analysis. Furthermore, an examination of different lithofacies is conducted to further analyze the factors influencing carbonate reservoir heterogeneity. These studies are essential for understanding the primary control factors of the development of reservoirs and may provide valuable support for gas exploration.

2 Geological background

The Ordos Basin is located on the western edge of North China, which is divided into six tectonic units, namely, the Yimeng Uplift in the north, the Jinxi flexure fold zone in the east, the Weibei Uplift in the south, the Tianhuan depression and the Xiyuan obduction zone in the west, and the Yishan Slope in the center (Figure 1A; Tu et al., 2016; Yang et al., 2022). The Lower Paleozoic natural gas production layer primarily lies at the top of the Ordovician weathering crust and the subsalt dolomite reservoir beneath the thick gypsum salt rock (Xiong et al., 2020; Meng et al., 2023). The Majiagou Formation was formed in the late Ordovician and is subdivided into O_1m_1 to O_1m_6. The lithology of the Majiagou Formation alternates between carbonate rocks and gypsum salt rock, among which the evaporite rocks in O_1m_1, O_1m_3, and O_1m_5 are limited to terrace-phase deposition in the sea-retreating cyclic platform, and the lithology is mainly salt rock, hard gypsum rocks, and thin layers of gypsum dolomite, muddy dolomite, and limestone (Xiong et al., 2020; Wang et al., 2022). On the other hand, O_1m_2, O_1m_4, and O_1m_6, deposited during the carbonate platform phase of the marine erosion cyclone, mainly consist of limestone and dolomite. The O_1m_5 Formation is $O_1m_5^{10\text{-}1}$ divided into 10 subsections by cyclical lithological characteristics and depositional sequences (Yang et al., 2022; Jiangmin et al., 2023).

Here, the study area is located in the south of the Yishan Slope of the Ordos Basin (Figure 1A), and we focus on $O_1m_5^{2-3}$ the formation, which is also known as "weathering crust" (Figure 1B). The lithology is dominated by argillaceous dolomite, fine silty crystalline dolomite crystalline dolomite in the $O_1m_5^3$ formation, and dolomite mainly developed during $O_1m_5^2$ the period (Cao et al., 2021).

3 Experiments and methods

3.1 Samples

The research samples were taken from the continuous core profile of the $O_1m_5^{2-3}$ Ordovician Formation in well A1. A total of eight carbonate core samples were collected for petrographic observation and the high-pressure mercury injection experiment (HPMI). These samples location are marked with red arrows (Figure 1B).

3.2 Petrographic observation

A total of 39 thin plates were polished for petrographic observation, of which eight thin sections were made from the core sample of well A1, and the 31 other thin sections were collected in the Natural Gas Research Institute of Shaanxi Yanchang Petroleum Group Co., LTD. The data images were collected by Xi'an Alberta Environmental Analysis and Testing Company. According to the Chinese Petroleum and Natural Gas Industry Standard SY/T 5368-2016, the mineral composition, particle type and content, and reservoir space classification were identified using a 59XC-PC polarizing microscope.

3.3 Petrophysical property tests

Petrophysical property tests of eight core samples were conducted, including the contents of porosity and permeability. The experiment was conducted at Xi'an Alberta Environmental Analysis and Testing Laboratory. The KX-07D gas porosity tester and the DX-07G gas permeability tester were used to collect porosity and permeability data and test procedures according to the Chinese Industry Standard GB/T 29,172-2012. In addition, we collected

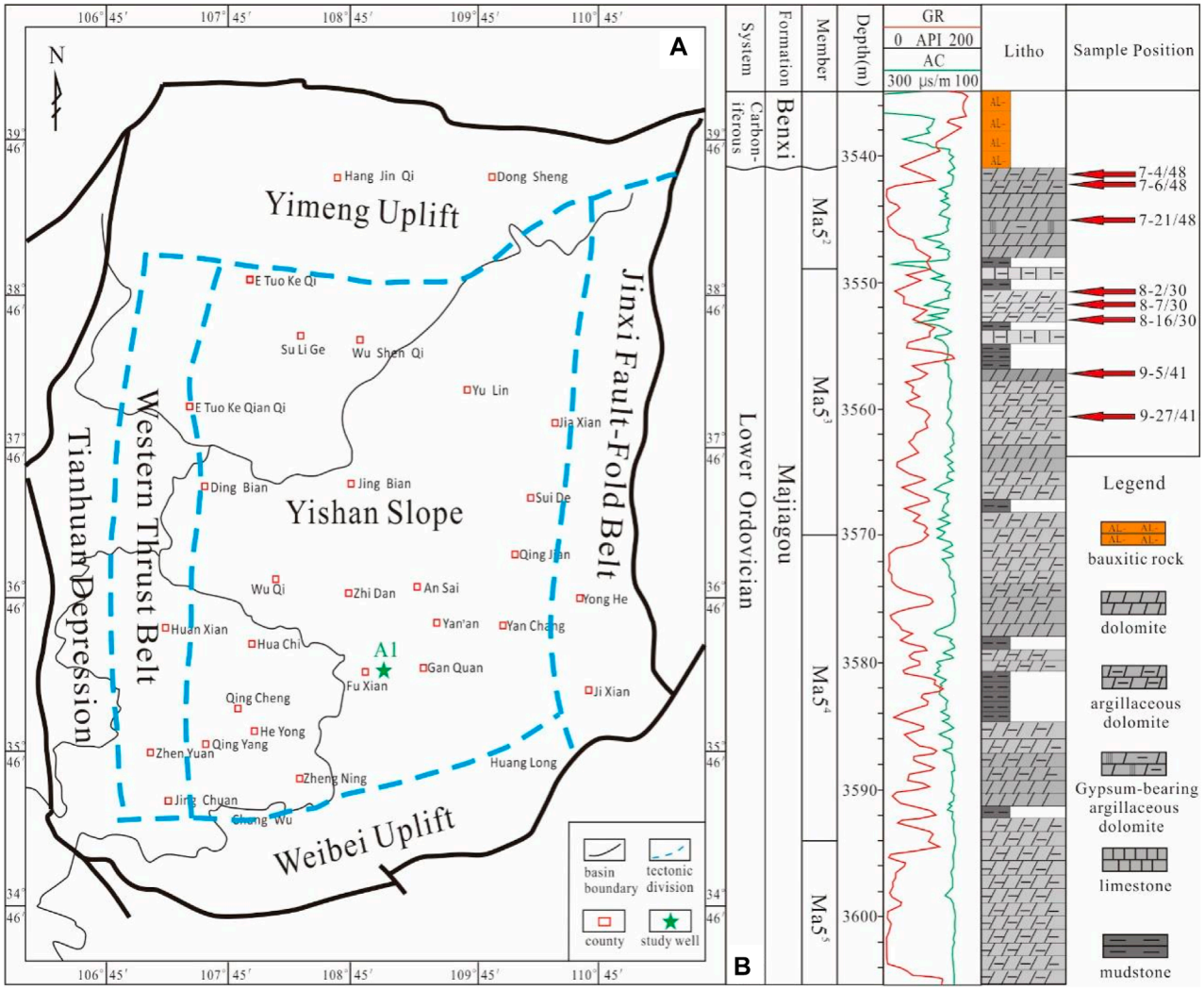

FIGURE 1
(A) Structural characteristics and the location of core well in the Ordos Basin and **(B)** the column of lithology characteristics and the sampling location.

31 porosity and permeability data from the natural gas research institute, Shaanxi Yanchang Petroleum Group Corporation.

3.4 High-pressure mercury injection

Pore structures and pore-size distributions of dolomite core samples were characterized via the HPMI technique. In the experiment, the Micromeritics AutoPore IV 9505 pore analyzer was used, and the maximum mercury injection capillary pressure was approximately 117 Mpa. Figure 5A presents mercury injection capillary pressure curves of all the core samples. Mercury is non-wetting on rock surfaces and has a high surface tension with air. With the mercury injection pressure increasing, non-wetting mercury enters the small pores of the core samples, and the pore radius can be calculated from the Eq. 1 in Washburn (1921):

$$P_c = \frac{2\sigma\cos\theta}{r}, \tag{1}$$

where P_c is the mercury injection capillary pressure; r is the pore radius; σ is the interfacial tension between mercury and air; and θ represents the mercury and rock contact angle. Under the maximum injection pressure, the corresponding minimum pore radius that can be detected is 6.3 nm. The structures and distributions of almost the entire pores, from nanoscale pores to microscale pores, were tested during the HPMI test, and then, the parameters of the pore structure were calculated from HPMI curves, as shown in Table 1.

According to the theory of fractal geometry, the fractal dimension via HPMI from Eq. 2, and it can be expressed by the log-log coordinate (Qu et al., 2022).

$$lg\left(1 - S_{Hg}\right) = (D-3) \times lg\left(P_c\right) - (D-3) \times lg\left(P_{min}\right), \tag{2}$$

where D is the fractal dimension; S_{Hg} is the mercury saturation; and P_c is the capillary pressure (Mpa). The fractal dimension was calculated from Eq. 3.

$$D = 3 + \mathrm{A}. \tag{3}$$

TABLE 1 Parameters of the pore–throat structure of the studied samples derived from HPMI experiments.

Sample ID	Entry pressure (MPa)	Average radius (μm)	Sorting coefficient	Maximum mercury saturation (%)	Efficiency of mercury withdrawal (%)	Skewness
7-21/48	12.854	0.009	0.020	20.680	26.614	3.409
8-2/30	10.305	0.010	0.020	20.000	20.500	4.334
8-7/30	12.816	0.011	0.014	21.400	17.757	4.334
7-4/48	15.345	0.004	0.008	20.900	26.334	3.050
9-5/41	14.097	0.003	0.006	20.914	23.596	2.892
8-16/30	5.120	0.015	0.030	29.711	8.212	6.461
7-6/48	16.013	0.002	0.004	13.529	9.565	3.657
9-27/41	9.846	0.002	0.006	14.706	19.317	3.645

The closer the value of D is to 2, the more regular the pore shape, whereas values of D closer to 3 account for a more complex pore structure (Wu et al., 2019).

If the weights of pore throats in different scales are w_1 and w_2, respectively, and the corresponding fractal dimensions are D1 and D2, then, as shown in Eq. 4

$$w_1 + w_2 = 1. \tag{4}$$

By weighting the fractal dimensions of pore throats in different scales, the total fractal dimensions (D) of the entire pore space can be calculated from Eq. 5 as follows (Qi et al., 2020):

$$D = D1 \times w_1 + D2 \times w_2. \tag{5}$$

4 Results

4.1 Petrophysical properties

Petrophysical properties, including porosity and permeability, are important parameters for evaluating reservoir characteristics (Henares et al., 2016; Zhang et al., 2018). The porosity and permeability of 39 samples vary widely across the study area. The porosity results range from 0.4% to 5.26%, with an average of 1.63% (Figure 2A). The permeability results range from 0.011 mD to 0.059 mD, with an average of 0.03 mD (Figure 2B). The result shows that these carbonate rocks of the study area are quite tight (porosity <5%, permeability <1mD). This is supported by the cast thin-section analysis, which is presented in the following section. In addition, there are relatively positive relationships between porosity and permeability (Figure 2C), reflecting that the carbonate reservoir is primarily pore-type and has moderate connectivity of the pore structure (Lai et al., 2019).

4.2 Petrology and reservoir space from the cast thin section

Considering the particle size characteristics, combined with observations and statistics of casting thin sections, the carbonate rock in the study area varies from argillaceous dolomite to fine silty crystalline dolomite to crystalline dolomite, according to Lai et al.'s (2013a) classification scheme.

Argillaceous dolomite is a dark gray, massive dolomite with predominantly 5 μm–20 μm-sized crystals, occasionally exhibiting horizontal bedding and micro-fracture (Figure 3A). The mineral composition consists mainly of micrite dolomite and argillaceous material, with the localized presence of gypsum (Figure 3B). Gypsum content is <10%, with the presence of a small amount of fine-grained quartz particles. Fine silty crystalline dolomite primarily ranges in size from 20 μm to 40 μm, displaying numerous micro-fractures approximately 20–200 μm wide. These micro-fractures are filled with sparry calcite (Figure 3C) or organic matter (Figure 3D) and exhibit some dissolution pores. Crystalline dolomite is a light brown crystalline dolomite comprising a mosaic of dolosparite crystals. It features a medium-coarse-grained, secondary, crystalline texture (Figure 3E), with crystal sizes ranging from 50 μm to 200 μm in size, and intergranular pore and intergranular dissolution pore can be observed as well (Figure 3F).

Observations of cast thin sections show that different degrees of dolomitization and karst transformation constitute the reservoir space of the Majiagou Formation, which is mainly composed of intra-crystalline pores (Figures 4A, B), intra-crystalline dissolved pores (Figure 4C), dissolved pores (Figures 4D–F), and micro-fractures (Figures 4G, H); the pores are partially filled with calcite (Figure 4I), and the primary pores are rare. The reservoir space varies from petrological characteristics. In contrast, few dissolution pores are observed in the argillaceous dolomite, indicating that lithology is the material basis for penecontemporaneous karstification. The dissolution capacity is determined by the clay content and structural composition. Generally, carbonate

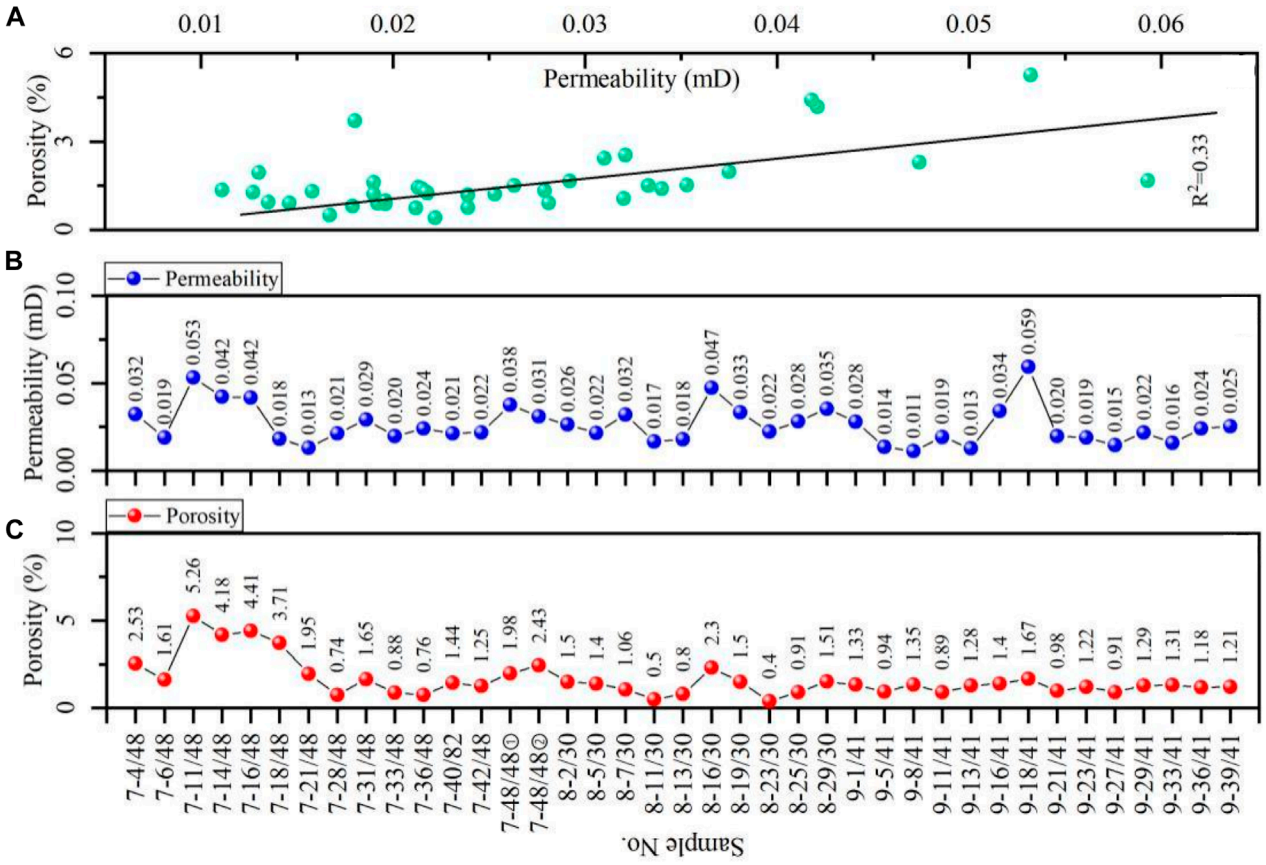

FIGURE 2
Petrophysical properties of the dolomite reservoir in the study area: **(A)** porosity results; **(B)** permeability results; **(C)** the correlation between porosity and permeability.

reservoirs with high clay content are not easy to be dissolved (Fu et al., 2012; Chen et al., 2016).

4.3 High-pressure mercury injection

HPMI tests are commonly used to study microscopic pore structures. Valuable information related to the microscopic pore structure of the reservoir can be obtained from HPMI curves, including pore type, pore–throat-size distribution, pore volume, average pore–throat radius, sorting coefficient, skewness, and withdraw efficiency (Chalmers G. R. L. et al., 2012; Clarkson and Williams-Kovacs, 2013; Juri et al., 2016; Lai et al., 2018).

According to Table 1, the displacement pressure for the reservoir, derived from the HPMI results, generally ranges from 5.12 to 15.15.35MPa, with an average of 12.05 MPa. The average pore–throat radius ranges from 0.002 μm to 0.015 μm, with an average of 0.007 μm. The sorting coefficient ranges from 0.004 to 0.03, with an average of 0.007, and the skewness ranges from 2.89 to 6.46. The maximum mercury saturation ranges from 13.53% to 29.71%, and the efficiency of mercury withdrawal ranges from 8.21% to 26.61%, with an average of 18.98%. The above characteristics reflect a complex and heterogeneous pore structure in the formation. In addition, mercury intrusion and extrusion curves are relatively isolated, and the mercury extrusion efficiency is low, which indicates considerable differences in the pore and throat sizes.

The HPMI curves varied by pore structure characteristics (Luo et al., 2008; Jiang et al., 2016). On the whole, the capillary curves lack an apparent horizontal stage in mercury intrusion (Figure 5), indicating general storage and permeability capacity (Piechaczek and Pusz, 2015; Mendhe et al., 2017). In detail, three types of HPMI curves could be identified based on the characteristics of the mercury intrusion curves. As shown in Figure 5A, type I and type III are represented by red and green solid dots, respectively, and smaller pore throats dominate the pore networks, making it difficult for mercury to pass through the pores, which have a markedly steep and almost horizontal stage in a mercury intrusion process. However, the mercury saturation of type III is less than that of type I, indicating the small pore volume and pore size. These blue series solid dots represent type II, which exhibit a relatively horizontal stage, with a gentle slope in the intermediate stage of the mercury intrusion process. This indicates that the micro-fractures developed with relatively better permeability.

The pore–throat size is considered one of the most crucial parameters in controlling the reservoir quality. The pore–throat size distribution and permeability contribution curves shown in Figure 5B, C are obtained from the HPMI test. Generally,

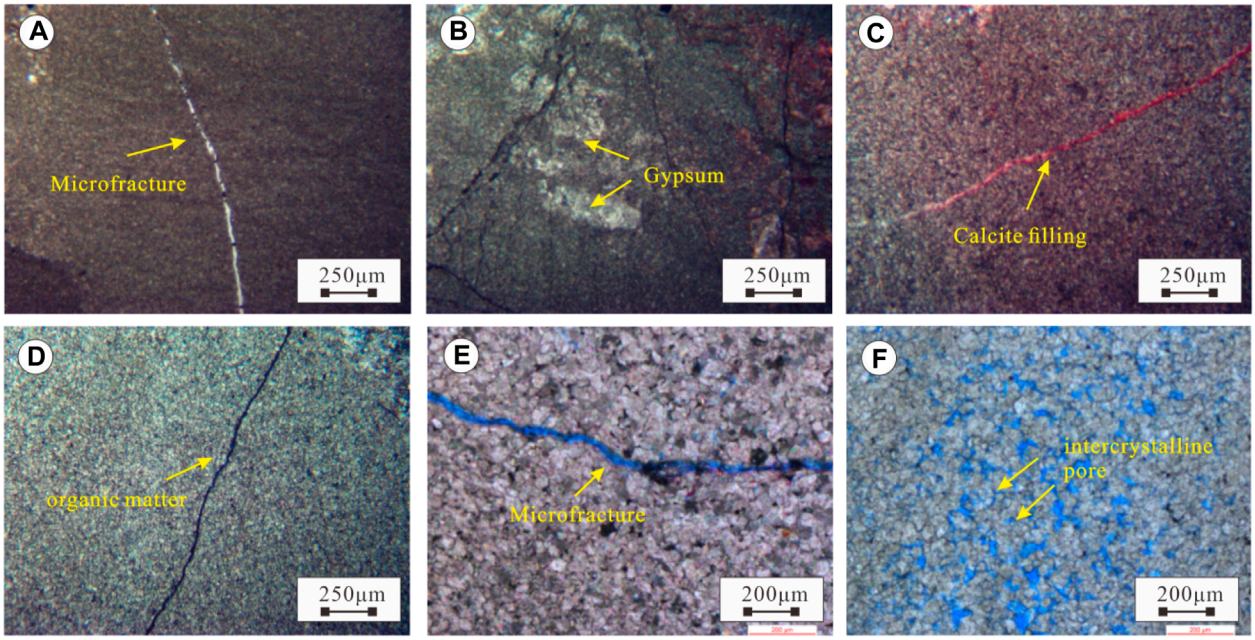

FIGURE 3
Petrologic characteristics of dolomite reservoirs for the Majiagou Formation: **(A)** argillaceous dolomite, 3,541.7 m; **(B)** gypsum-bearing argillaceous dolomite, 3,545.7 m; **(C)** fine silty crystalline dolomite, calcite filling, 3,553.9 m; **(D)** fine silty crystalline dolomite, organic matter filling, 3,550.3 m; **(E)** crystalline dolomite, 3,560.8 m; and **(F)** crystalline dolomite with interpores developed, 3,563.3 m.

the pore–throat size distribution of each sample exhibits a unimodal pattern, with pore–throat radii predominately ranging from 0.006 μm to 0.02 μm and 0.04 μm–0.15 μm. Additionally, the type I pores are numerous but small, type II pores are few but large, and type III pores are both few and small in size. The permeability contribution curve also demonstrates a unimodal distribution, with similar maximum permeability contributions for different reservoir types, as depicted in Figure 5C. The permeability values for type I, type II, and type III are 2.3%–46.19%, 1.06%–51.29%, and 1.5%–44.83%, respectively, with average values of approximately 19.47%, 20.53%, and 19.36%. Notably, the difference lies in that the permeability is primarily provided by the small pores of type I and type III, while it is mainly contributed by the large pores of type II. In addition, maximum mercury saturation serves as an important parameter reflecting pore connectivity. The results indicate that the maximum mercury saturation value is low for type III, while the values of type I and type II are similar (Figure 5D). In summary, type I exhibits more pore throats and rather good permeability contribution compared to type II and type III.

4.4 Fractal characteristics

The fractal dimension (D) deduced from fractal theory can quantitatively evaluate pore surface roughness and structural irregularity, which is an important parameter for reservoir heterogeneity evaluation (Piechaczek and Pusz, 2015; Jiang et al., 2016; Norbisrath et al., 2016; Mendhe et al., 2017). It is consensus that using HPMI data is an effective method to compute fractal dimensions of various reservoirs (e.g., Angulo et al., 1992; Li and Horne, 2006; Li, 2010). Therefore, we use the basis of HPMI data to calculate fractal dimensions of pores in carbonate reservoirs.

As shown in Figure 6, all the linear models demonstrate a strong fit with coefficients (R^2) ranging from 0.96 to 0.998 (Table 2), indicating that these carbonate samples exhibit fractal characteristics and can be effectively described by using fractal geometry theory. The calculations reveal that a larger fractal dimension corresponds to stronger reservoir heterogeneity, aligning with previous research findings (Jiang et al., 2016; Lai et al., 2019). The plot of fractal characteristics for all samples can be segmented into two parts. Here, we calculated D1 and D2 for each segment and also computed weighted D for each sample by using formula 4 and formula 5. The result shows that the values of D1 range from 2.87 to 2.97, with an average of 2.91, and the values of D2 range from 2.71 to 2.96, with an average of 2.86, indicating strong heterogeneity in large pores. In addition, the fractal characteristics vary depending on the types of reservoirs. The average values of D in type I, type II, and type III are 2.87, 2.92, and 2.82, respectively. As shown in Figures 6A–C, the slope for the small pore–throats is slightly steeper than that for the large pore–throats in type I reservoir, and the average fractal dimension of D1 and D2 is 2.89 and 2.86, respectively. There is little difference between D1 and D2, indicating the homogeneity of pores is almost the same for different pore sizes. The average fractal dimensions of D1 and D2 in type II are 2.90 and 2.94, respectively (Figures 6D–F), and the average dimensions of D1 and D2 in type III are 2.87 and 2.71, respectively, (Figures 6G, H). The fractal dimension of type II is generally larger than that of type III, and the heterogeneity of larger pores in type II is stronger than that of small pores, while it is opposite in type III. It was observed that compared with the three types mentioned above, the

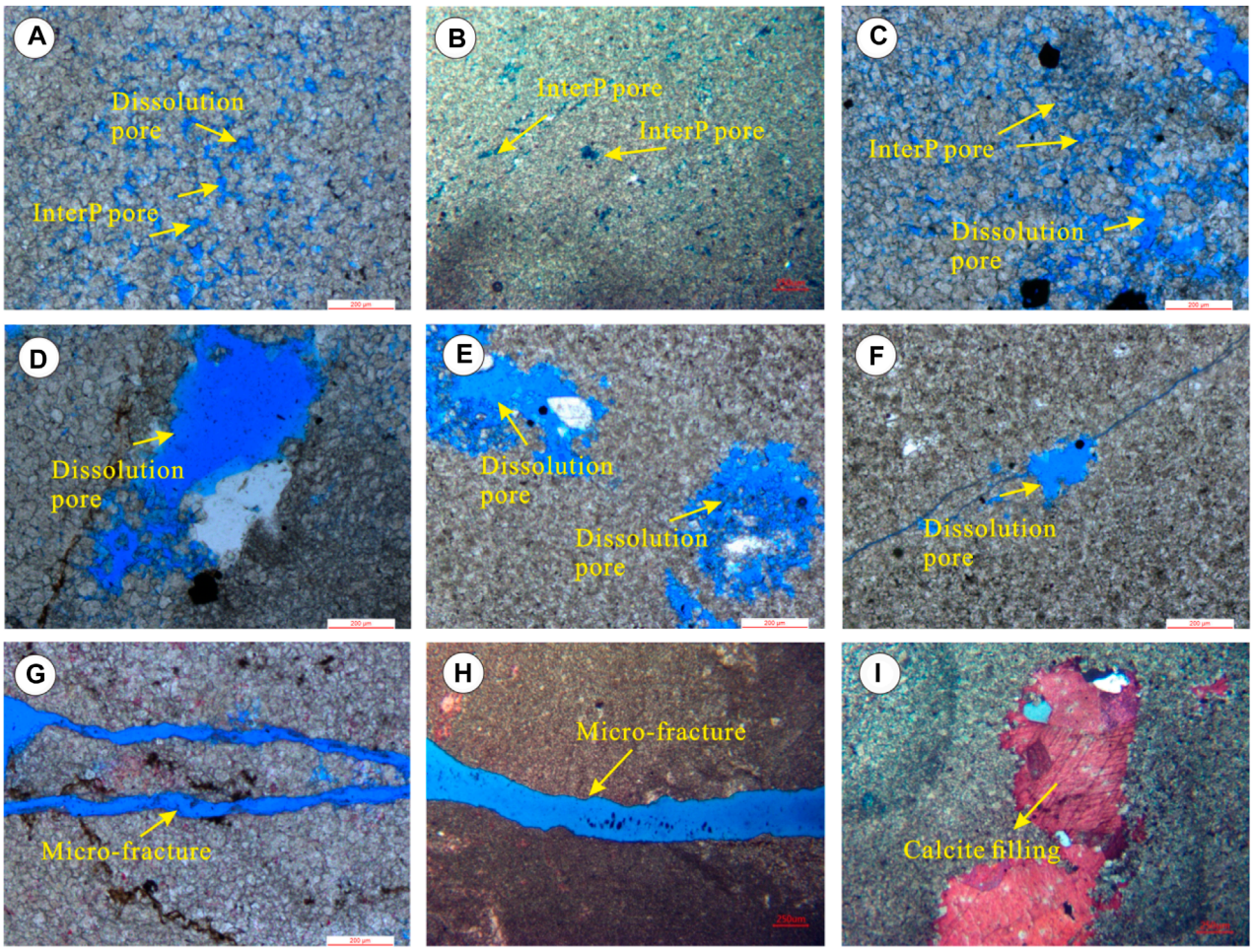

FIGURE 4
Pore characteristics of the dolomite reservoir in the study area: **(A)** interP pore and dissolution pore in crystalline dolomite, 3,563.3 m; **(B)** interP pore, 3,545.8 m; **(C)** interP pore and dissolution pore, 3,560.8 m; **(D)** dissolution pore, 3,559.7 m; **(E)** dissolution pore, 3,560.3 m; **(F)** dissolution pore and micro-fracture, 3,587.3 m; **(G)** micro-fracture in fine silty crystalline dolomite, 3,552.6 m; **(H)** micro-fracture in argillaceous dolomite, 3,541.7 m; and **(I)** dissolution pore is filled by calcite, 3,543.6 m.

value of fractal dimension in type I is low, and it exhibits nearly uniform heterogeneity across different pore sizes, which contributes significantly toward storage capacity and permeability.

5 Discussion

5.1 Relationship between fractal dimension, porosity, and permeability

Porosity and permeability are considered the two most important parameters for evaluating reservoir properties. As shown in Figure 7A, porosity demonstrates a week negative correlation with fractal dimension, with a coefficient of 0.22. Permeability reflects the ability of rock to allow fluid to flow through its pores and exhibits a relatively weak positive relationship with fractal dimension, having a coefficient of 0.28 (Figure 7B). A higher fractal dimension implies a transformation of pore morphology from regular to complex and the pore surface from smooth to rough, resulting in reduced porosity and permeability (He et al., 2016; Li et al., 2017). However, the positive relationship between permeability and fractal dimension is uncommon, necessitating further classification analysis.

Additionally, the correlation between porosity and permeability with fractal dimension in different reservoir types is examined. The samples were divided into two parts based on the comparison of D1 and D2 values: D1 is larger than D2 in type I and type III reservoirs, while D1 is smaller than D2 in type II reservoirs. The results indicate a negative correlation between porosity (Figure 7C) and permeability (Figure 7D) with fractal dimension with different reservoir types, aligning with the general consensus (Chalmers G. R. et al., 2012; Amosu et al., 2018). In tight reservoirs containing numerous pores with small size, irregularly distributed small pores with high fractal dimensions may inhibit the development of larger pores, leading to reduced porosity (Shao et al., 2017). Small-sized pores exhibit strong heterogeneity in type II reservoirs; therefore, despite having large values of porosity and permeability, the reservoir quality remains poor.

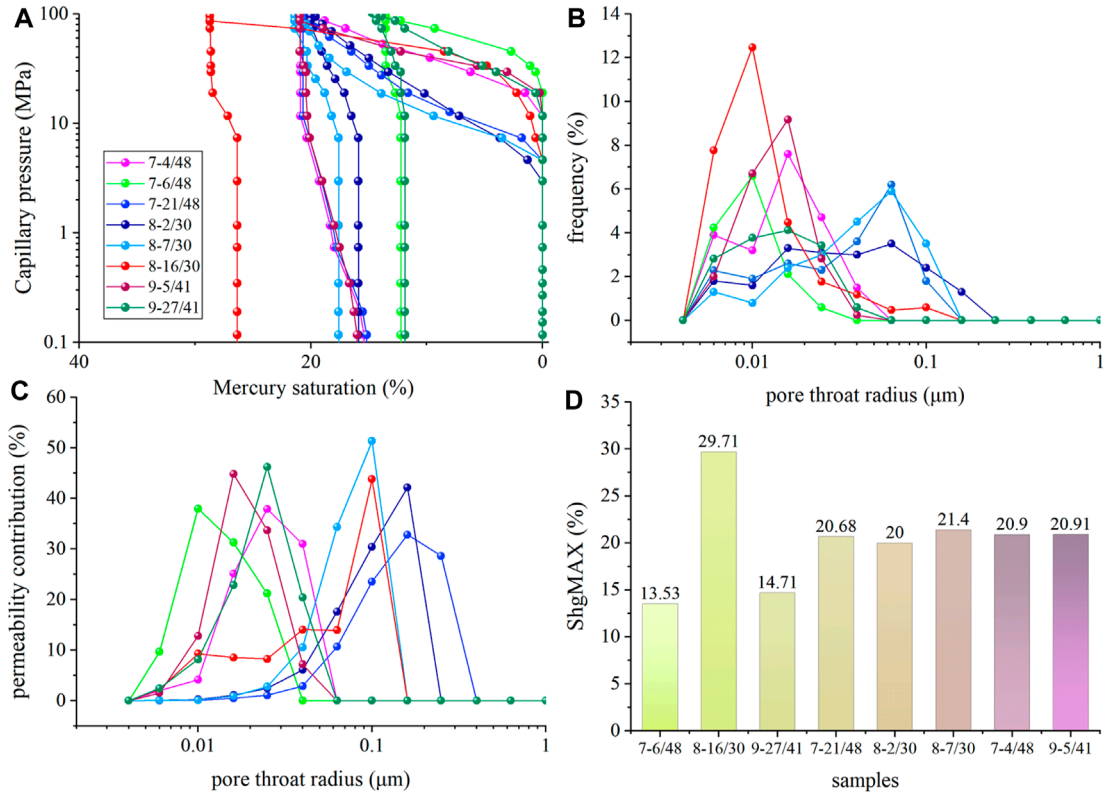

FIGURE 5
(A) Capillary pressure curves, **(B)** pore-size distribution, **(C)** permeability contribution curve, and **(D)** histogram of maximum mercury injection obtained by performing the HPMI experiments. Red, blue, and green series solid dots represent type I, type II, and type III, respectively.

5.2 Relationship between the fractal dimension and pore structure parameters

A series of plots were produced to investigate the relationships between pore structure parameters (i.e., entry pressure, average pore throat radius, sorting coefficient, mercury withdraw efficiency, maximum mercury saturation, and skewness) and fractal dimension, as shown in Figure 8. There are outliers (solid blue dots), which are different from other samples as they have a large number of micropores. Beyond that, other samples have considerable correlation with fractal dimensions, which provides a source of evidence for reservoir evaluation analysis. As shown in Figure 8A, the entry pressure indicates the pore size (Chen et al., 2018); there is negative relationship between entry pressure and fractal dimension, that is, the smaller the pore size, the lower the heterogeneity. This is because the pores with the smaller size in the reservoir are mostly intercrystalline pores with good homogeneity (Figure 4A), while the large pores are mostly dissolution pores with irregular shapes and strong heterogeneity (Figure 4E). The average pore–throat radius shows a moderate positive correlation with fractal dimensions (Figure 8B). This may be attributed to the development of dissolution pores or micro-fractures with large pore sizes and strong heterogeneity (Figure 4G). Additionally, Figure 8C illustrates a positive correlation between the sorting coefficient and fractal dimension, with a coefficient of 0.72. It indicates that as the sorting coefficient increases, the fractal dimension increases and the pore structure becomes more complex, enhancing the heterogeneity of the pore structure. Figure 8D shows a very slightly positive relationship between the efficiency of mercury withdrawal and fractal dimension, which indicates a considerable number of micropores generated in the strong heterogeneous samples. This is because due to the complexity of the reservoir, although the sample with a large pore volume mainly develops macropores, the value of the micropore volume is also very considerable. Maximum mercury saturation reflects pore connectivity. In general, the maximum mercury saturation increases with the increase in the pore volume (Zhang et al., 2018), but the strong heterogeneity of large pores generated, which reduces the connectivity to some extent (Figure 8E). Skewness is a pore structure parameter that reflects the distribution of pore–throat sizes. The moderately positive correlation between the skewness value and the fractal dimension suggests that large pore–throats are predominant in the pore networks (Figure 8F), which results in a high fractal dimension. In general, the fractal dimensions demonstrate relatively strong correlations with pore structure parameters, making it a valuable metric for quantitatively characterizing carbonate properties and complexity of pore networks.

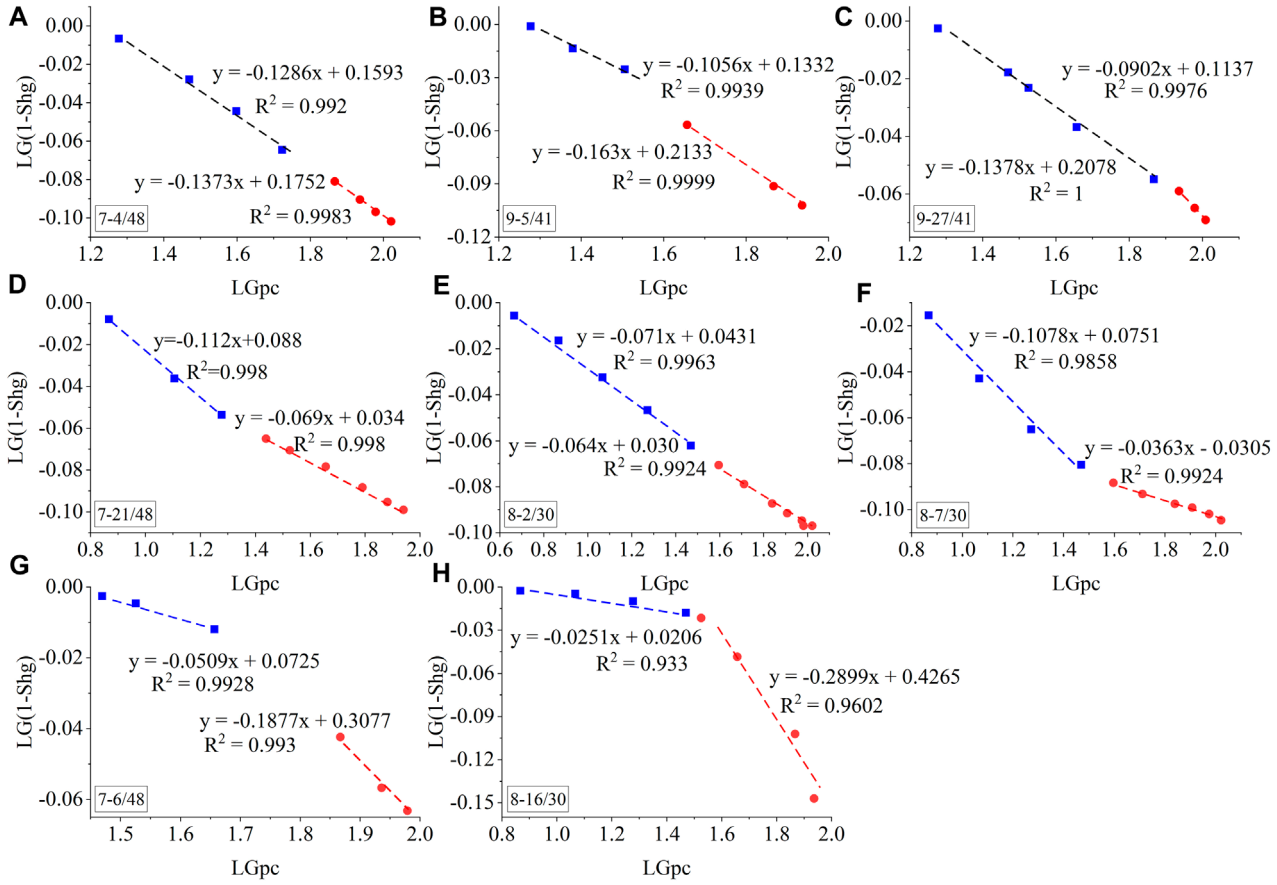

FIGURE 6
Fractal dimension curve of **(A–C)** type I, **(D–F)** type II, and **(G, H)** type III.

TABLE 2 Fractal dimensions of eight carbonate samples derived from HPMI data.

Type	Sample ID	K_1	R_1^2	D_1	K_2	R_2^2	D_2	D
Type I	7-4/48	−0.13	0.992	2.87	−0.14	0.998	2.86	2.87
	9-5/41	−0.11	0.994	2.89	−0.16	0.999	2.84	2.85
	9-27/41	−0.09	0.997	2.91	−0.14	1	2.86	2.90
Type II	7-21/48	−0.11	0.998	2.89	−0.06	0.998	2.94	2.91
	8-2/30	−0.07	0.996	2.93	−0.06	0.992	2.94	2.93
	8-7/30	−0.11	0.986	2.89	−0.04	0.992	2.96	2.90
Type III	7-6/48	−0.05	0.993	2.95	−0.19	0.933	2.81	2.84
	8-16/30	−0.03	0.993	2.97	−0.29	0.96	2.71	2.90

5.3 Relationship between diagenesis and the pore structure

The formation in the study area is dominated by karst dolostone (Yang et al., 2022), and the XRD results show that the mineral component content of different samples is similar, that is, the dolomite content ranges from 93% to 89%, with an average content of 91.4% (Wu et al., 2023), so it is not appropriate to divide lithofacies based on the mineral composition content. Diagenetic facies are a comprehensive characterization of diagenesis,

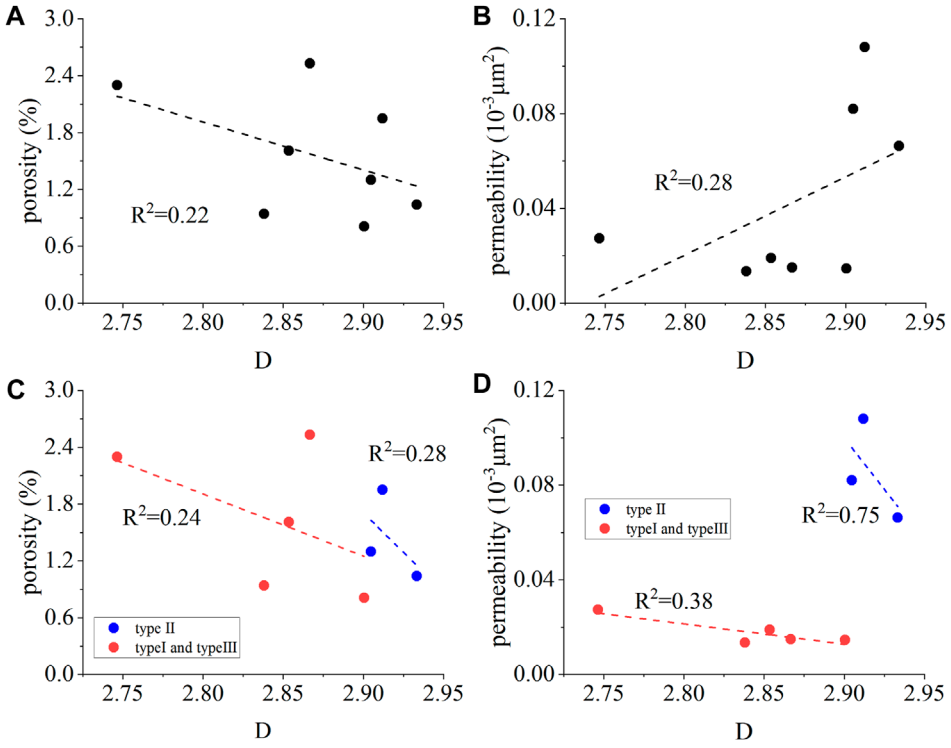

FIGURE 7
Relationship of fractal dimension with **(A, C)** porosity and **(B, D)** permeability.

reservoir physical properties, types, and advantages, which is widely used to classify carbonate reservoirs (Lai et al., 2013a; Lai et al., 2013b; Zhang et al., 2010; Zou et al., 2008). Reservoir classification based on diagenetic facies requires a large number of thin-section observations, which is qualitative analysis, and the results are affected by human factors. However, due to the number of samples, the classification method based on diagenetic facies is not applicable. In addition, the pores are formed by different types of diagenesis, and the sizes of different types of pores are different (Wang et al., 2023). Furthermore, the thin section, petrophysical property, and HPMI can be qualitatively and quantitatively characterized, making them suitable for the classification of carbonate reservoirs in the study area. Therefore, we establish pore structure facies using the capillary pressure curves, pore-size distribution, reservoir permeability contribution, and fractal dimension from mercury injection experiments, and consider diagenesis from casting thin section observations to illustrate the effect of diagenesis on different types of pore structures.

5.3.1 Micro-porous facies

The limited number of intercrystalline pores is a result of dolomitization, calcite cementation, and dissolution in the micro-porous facies (Figure 9E). The low mercury saturation (Figure 9A) and some dissolved pores can be observed in the cast thin section (Figure 9D). These facies exhibit poor reservoir property, with small pore–throat sizes (dominated by pore throat between 0.007 μm and 0.01 μm), contributing to its low permeability capacity, mainly provided by small channels connecting intercrystalline pores (Figure 9B). Furthermore, the fractal plot of this type of reservoir is divided into two segments, where D1 is larger than D2 (Figure 9C), indicating strong heterogeneity with larger pore sizes. Overall, the micro-porous facies exhibits low porosity properties and poor permeability.

5.3.2 Intra-crystalline (dissolved) pore facies

These facies are characterized by intra-crystalline pores (Figure 4B), dissolved pores, and micro-fractures (Figure 9I; Figure 4I). Micro-fractures are effective channels for fluid flow in reservoirs, promoting the dissolution of soluble components during fluid passage, which is beneficial for improving reservoir permeability. However, the analysis of the capillary pressure curve and deduced data (Figure 9F) indicates a relatively small pore number and pore size with the diameter between 0.04 μm and 0.08 μm, resulting in a relatively weak storage capacity (Figure 9g). Additionally, the fractal plot of this reservoir type exhibits two segments, with D1 smaller than D2 (Figure 9H), indicating the strong heterogeneity in small pore-size distribution. Generally, micro-fractures are prevalent in the facies, leading to unevenly distributed pores due to calcite cementation, which contributes to permeability but limits storage capacity.

5.3.3 Corrosion pore facies

The corrosion facies exhibits dissolved pores, intra-crystalline pores, and few micro-fractures (Figure 9N). Penecontemporaneous

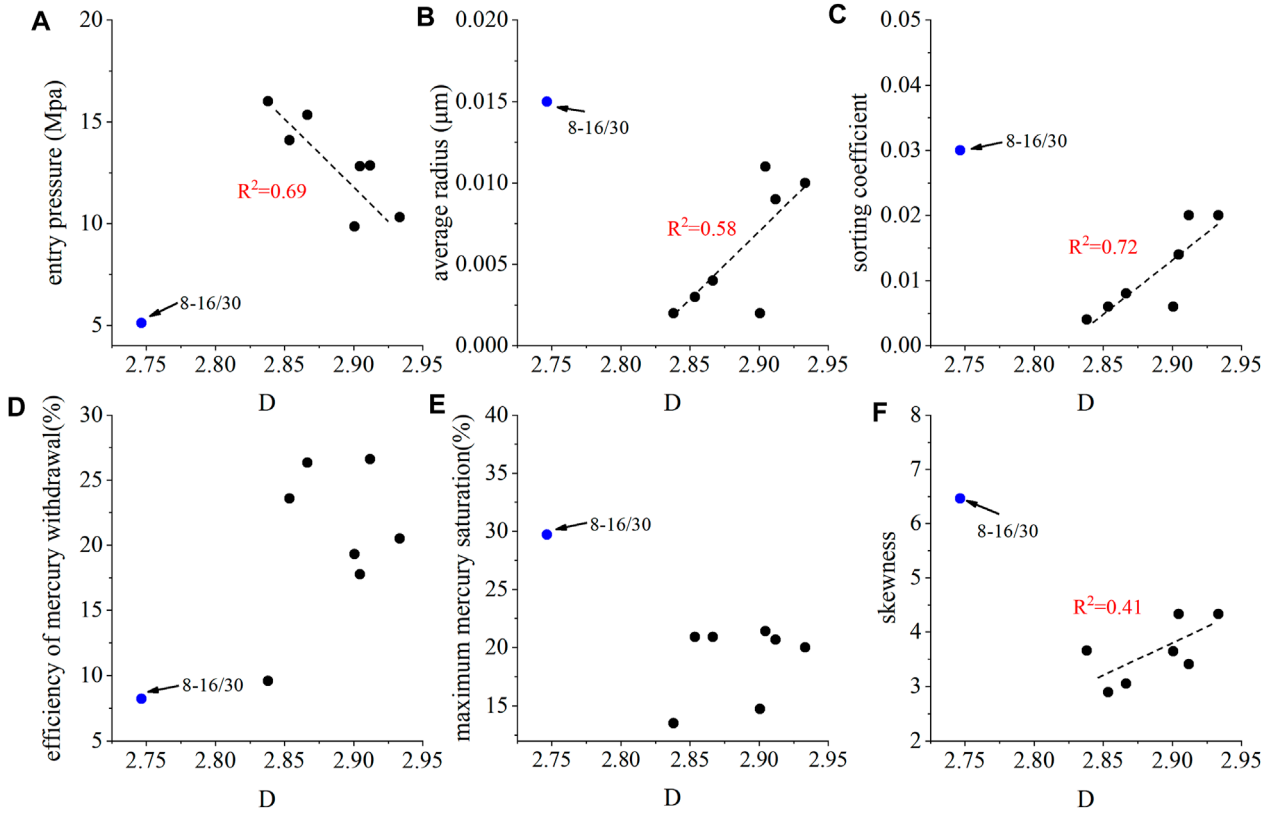

FIGURE 8
Relationships of fractal dimension with **(A)** entry pressure, **(B)** average pore–throat radius, **(C)** sorting coefficient, **(D)** efficiency of mercury withdrawal, **(E)** maximum mercury saturation, and **(F)** skewness.

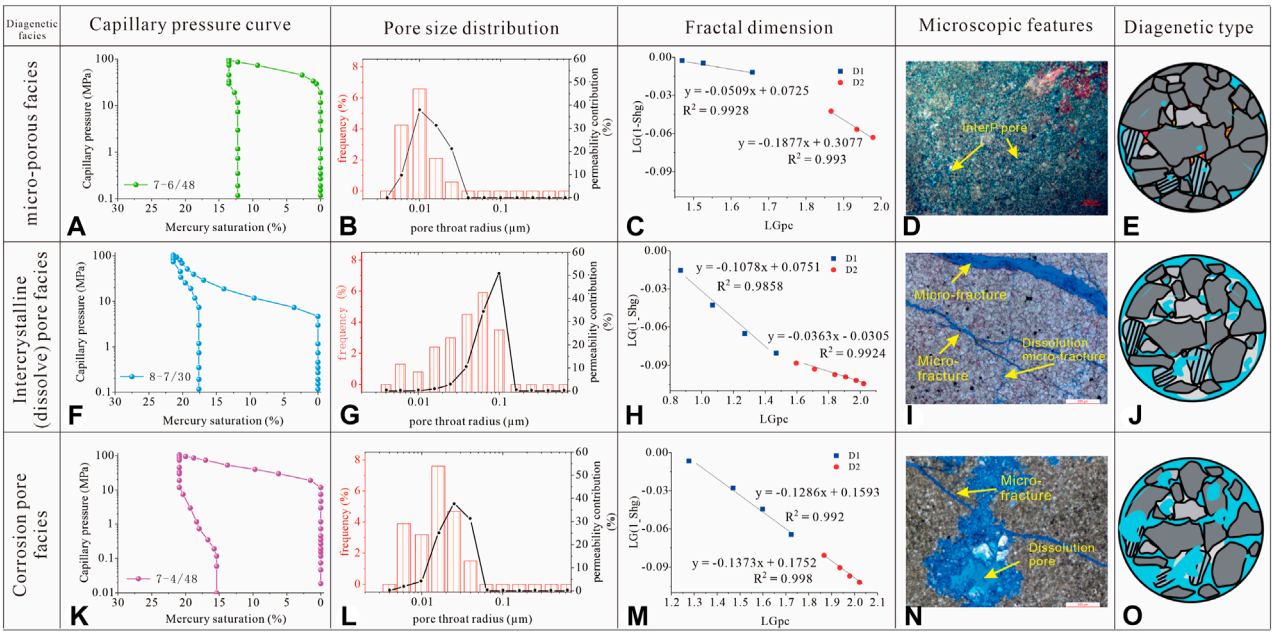

FIGURE 9
The characteristics of micro-porous facies are **(A)** low mercury saturation, **(B)** small pore size, **(C)** D1 is larger than D2, **(D)** interP pores developed with **(E)** compaction. The Intra-crystalline (dissolved) pore facies with **(F)** high mercury saturation, **(G)** big pore size, **(H)** D1 smaller than D2, and **(I)** dissolved pores and micro-fracture developed when **(J)** dissolution. Corrosion pore facies have **(K)** high mercury saturation, **(L)** relatively big pore size, **(M)** relatively strong heterogeneity, **(N)** dissolved pores, intra-crystalline pores, and few micro-fractures developed through **(O)** penecontemporaneous karstification.

karstification transforms intergranular pores into dissolution pores, which is evident in the core observation as pinhole shapes (Figure 9O) (Xiong et al., 2020). Furthermore, dolomite can be dissolved by hydrogen sulfide produced through sulfate thermochemical reduction under weakly acidic conditions (Yu et al., 2012; Zou et al., 2008), resulting in common dissolution pores in fine silty crystalline dolomite and crystalline dolomite, but rarely in argillaceous dolomite. The reservoir's pore–throat radius mainly ranges from 0.01 μm to 0.03 μm, with the main permeability contribution coming from pore sizes of 0.02 μm–0.04 μm (Figure 9L). Additionally, the homogeneity of the pore structure across different pore sizes is better-illustrated (Figure 9M), along with high petrophysical properties indicating its potential prolific reservoirs.

6 Conclusion

In this study, we used various experimental methods and fractal theory to investigate the pore structure, fractal characteristics, and main controlling factors of the Majiagou Formation in the Ordos Basin. The key conclusions are summarized as follows:

(1) The dolomite reservoir of the Majiagou Formation in the Ordos Basin exhibits a development of argillaceous dolomite, fine silty crystalline dolomite, and crystalline dolomite with intra-crystalline pores, intra-crystalline dissolved pores, dissolved pores, and micro-fractures predominating.

(2) Based on the analysis of HPMI curves and petrophysical measurements, the reservoir was classified into three types: dissolved pore type, micro-fracture (intra-crystalline) pore type, and micro-porous type. The micro-porous type exhibits a small number of intra-crystalline pores with small pore–throat sizes. In contrast, the micro-fracture pore type displays developed micro-fractures and large pores but with a limited number of pores, indicating the good permeability but the poor storage capacity. The dissolved pore type is characterized by a significant quantity of dissolved pores along with few microfractures, resulting in a large pore volume and relatively better permeability.

(3) Fractal dimension analysis derived from the HPMI data reveals reservoir heterogeneity that can be segmented into two section categories varying across different types. Larger fractal dimensions observed for larger pores in the micro-porous type indicate the complex pore structure. The weighted average fractal dimensions in the micro-fracture (intra-crystalline) pore type and micro-porous type are 2.92 and 2.87, respectively, while it is 2.82 in the dissolved pore type. A lower value of the fractal dimension indicates a less heterogeneity of pore structure, which may have implications for the fluid flow and storage within the rock formation.

(4) The quantitative characterization of the pore structure in dolomite reservoirs is greatly facilitated by the measurement of fractal dimension, which exhibits positive correlations with porosity, permeability, and the pore structure parameter. Furthermore, the dissolved pore type, characterized by a large pore size and homogeneity structure, resulting from penecontemporaneous dolomitization and leaching due to meteoric freshwater ingress, is identified as a potentially prolific reservoir.

Data availability statement

The original contributions presented in the study are included in the article/Supplementary Material; further inquiries can be directed to the corresponding author.

Author contributions

KT: conceptualization, methodology, writing–original draft, and writing–review and editing. XQ: conceptualization, funding acquisition, supervision, and writing–review and editing. JZ: formal analysis, supervision, and writing–review and editing. CX: conceptualization, methodology, and writing–review and editing. JC: data curation and writing–review and editing. XY: supervision and writing–review and editing. SL: Project administration and writing–review and editing. BZ: Software and writing–review and editing.

Funding

The authors declare that financial support was received for the research, authorship, and/or publication of this article. The project received funding from the Key R&D Plan of Shaanxi Province: Intelligent Evaluation Technology for Tight Gas Reservoir Driven by Data Mechanism Hybrid (Projects #2023-YBGY-308) and Key R&D Plan of Shaanxi Yanchang Petroleum (Group) Co., Ltd: Research on Key Technologies for Reservoir Stimulation in the Zhidanxi-Wuqi Region (Projects #ycsy2022jb-A-03).

Conflict of interest

Authors KT, XQ, JZ, JC, XY, and BZ were employed by the Research Institute of Shaanxi Yanchang Petroleum Group Co., Ltd.

Author CX was employed by PetroChina Changqing Oilfield Company.

Author SL was employed by the Research Institute of Shaanxi Yanchang Petroleum Group Co., Ltd.

Publisher's note

References

Amosu, A., Mahmood, H., and Ofoche, P. (2018). Estimating the permeability of carbonate rocks from the fractal properties of moldic pores using the kozeny-carman equation. *Res. Ideas Outcomes* 4, e24430. doi:10.3897/rio.4.e24430

Angulo, R. F., Alvarado, V., and Gonzalez, H. (1992). "Fractal dimensions from mercury intrusion capillary tests," in SPE Latin America Petroleum Engineering Conference (Society of Petroleum Engineers).

Cao, H., Li, W., Wu, H., Wang, Z., Wu, Y., and Ren, X. (2021). Lithofacies palaeogeography evolution of the member 5 of ordovician Majiagou sedimentary stage in northern Shaanxi Province. *Journal of Palaeogeography*, 23 (4):723–734. doi:10.7605/gdlxb.2021.04.048

Chalmers, G. R., Bustin, R. M., and Power, I. M. (2012a). Characterization of gas shale pore systems by porosimetry, pycnometry, surface area, and field emission scanning electron microscopy/transmission electron microscopy image analyses: examples from the Barnett, Woodford, Haynesville, Marcellus, and Doig units. *AAPG Bull.* 96 (6), 1099–1119. doi:10.1306/10171111052

Chalmers, G. R. L., Ross, D. J. K., and Bustin, R. M. (2012b). Geological controls on matrix permeability of devonian gas shales in the horn river and liard basins, northeastern british columbia, Canada. *Int. J. Coal Geol.* 103 (23), 120–131. doi:10.1016/j.coal.2012.05.006

Chen, A. Q., Xu, S. L., Yang, S., Chen, H. D., Su, Z. T., Zhong, Y. J., et al. (2018). Ordovician deep dolomite reservoirs in the intracratonic Ordos Basin, China: depositional model and Diagenetic evolution. *Energy explor. Exploit.* 36 (4), 850–871. doi:10.1177/0144598718778171

Chen, H., Wu, Y., Zhu, H., Lu, Z., Cao, Z., and Yun, L. (2016). Eogenetic karstification and reservoir formation model of the Middle-Lower Ordovician in the northeast slope of Tazhong uplift, Tarim Basin. *Acta Pet. Sin.* 37 (10), 1231–1246. doi:10.7623/syxb201610003

Clarkson, C. R., and Williams-Kovacs, J. D. (2013). Modeling two-phase flowback of multifractured horizontal wells completed in shale. *Spe J.* 18 (04), 795–812. doi:10.2118/162593-pa

Fu, J., Bai, H., Sun, L., and Ma, Z. (2012). Types and characteristics of the ordovician carbonate reservoirs in Ordos Basin, China. *Acta Pet. Sin.* 33 (S2), 110–117.

Gane, P. A., Ridgway, C. J., Lehtinen, E., Valiullin, R., Furó, I., Schoelkopf, J., et al. (2004). Comparison of NMR cryoporometry, mercury intrusion porosimetry, and DSC thermoporosimetry in characterizing pore size distributions of compressed finely ground calcium carbonate structures. *Ind. Eng. Chem. Res.* 43 (24), 7920–7927. doi:10.1021/ie049448p

Gundogar, A., Ross, C., Akin, S., and Kovscek, A. (2016). Multiscale pore structure characterization of Middle East carbonates. *J. Petrol. Sci. Eng.* 146, 570–583. doi:10.1016/j.petrol.2016.07.018

He, J. H., Ding, W. L., Li, A., Sun, Y. X., Dai, P., Yin, S., et al. (2016). Quantitative microporosity evaluation using mercury injection and digital image analysis in tight carbonate rocks: a case study from the Ordovician in the Tazhong Palaeouplift, Tarim Basin, NW China. *J. Nat. Gas. Sci. Eng.* 34, 627–644. doi:10.1016/j.jngse.2016.07.025

Henares, S., Caracciolo, L., Viseras, C., Fernandez, J., and Yeste, L. M. (2016). Diagenetic constraints on heterogeneous reservoir quality assessment: a Triassic outcrop analog of meandering fluvial reservoirs. *AAPG Bull.* 100, 1377–1398. doi:10.1306/04011615103

Hulea, I. N., and Nicholls, C. A. (2012). Carbonate rock characterization and modeling: capillary pressure and permeability in multimodal rocks—a look beyond sample specific heterogeneity. *AAPG Bull.* 96 (9), 1627–1642. doi:10.1306/02071211124

Jiang, F. J., Chen, D., Chen, J., Li, Q. W., Liu, Y., Shao, X. H., et al. (2016). Fractal analysis of shale pore structure of continental gas shale reservoir in the ordos basin, NW China. *Energy Fuel* 30 (6), 4676–4689. doi:10.1021/acs.energyfuels.6b00574

Jiangmin, D. U., Zihao, C. U. I., Zhiwei, J. I. A., Yi, Z. H. A. N. G., Wancai, N. I. E., Yupeng, L. O. N G., et al. (2023). Sedimentary characteristics of Ma5 5 sub-member of ordovician Majiagou Formation in sulige area. *Ordos Basin Lithologic Reserv. 35* 5, 37–48. doi:10.12108/yxyqc.20230504

Jouini, M., Vega, S., and Mokhtar, E. (2011). Multiscale characterization of pore spaces using multifractals analysis of scanning electronic microscopy images of carbonates. *Nonlinear Process Geophys* 18 (6), 941–953. doi:10.5194/npg-18-941-2011

Juri, J. E., Dijke, M. I. J. V., and Sorbie, K. S. (2016). Inversion of the lattice network wettability subjected to the capillary pressure of the entire flooding cycle: Hamiltonian Monte Carlo posterior sampling and prediction of the relative permeability. *J. Petrol. Sci.Eng.* 146, 1037–1062. doi:10.1016/j.petrol.2016.07.006

Lai, J., Wang, G., Chen, M., Wang, S., Chai, Y., Cai, C., et al. (2013a). Pore structures evaluation of low permeability clastic reservoirs based on petrophysical facies: a case study on Chang 8 reservoir in the Jiyuan region, Ordos Basin. *Petroleum Explor. Dev.* 40 (5), 566–573. doi:10.11698/PED.2013.05.08

Lai, J., Wang, G., Wang, S., Zheng, X., Wu, H., and Zhang, Y. (2013b). Research status and advances in the diagenetic facies of clastic reservoir. *Adv. Earth Sci.* 28 (1), 39–50.

Lai, J., Wang, G., Wang, Z., Chen, J., Pang, X., Wang, S., et al. (2018). A review on pore structure characterization in tight sandstones. *Earth Sci. Rev.* 177, 436–457. doi:10.1016/j.earscirev.2017.12.003

Lai, J., Wang, S., Wang, G., Shi, Y., Zhao, T., Pang, X., et al. (2019). Pore structure and fractal characteristics of Ordovic-ian Majiagou carbonate reservoirs in Ordos Basin, China. *AAPG Bull.* 103 (3), 2573–2596. doi:10.1306/02251917173

Li, K. (2010). Analytical derivation of Brooks–Corey type capillary pressure models using fractal geometry and evaluation of rock heterogeneity. *J. Petrol. Sci. Eng.* 73 (1), 20–26. doi:10.1016/j.petrol.2010.05.002

Li, K., and Horne, R. N. (2006). Comparison of methods to calculate relative permeability from capillary pressure in consolidated water-wet porous media. *Water Resour. Res.* 42 (6). doi:10.1029/2005wr004482

Li, P., Zheng, M., Bi, H., Wu, S., and Wang, X. (2017). Pore throat structure and fractal characteristics of tight oil sandstone: a case study in the Ordos Basin, China. *J. Petrol. Sci. Eng.* 149, 665–674. doi:10.1016/j.petrol.2016.11.015

Luo, P., Zhang, J., and Liu, W. (2008). Characteristics of marine carbonate hydrocarbon reservoirs in China. *Earth Sci. Front.* 15 (1), 36–50.

Ma, Y. S., He, D. F., Cai, X. Y., and Liu, B. (2017). Distribution and fundamental science questions for petroleum geology of marine carbonate in China. *Acta Petrol. Sin.* 54 (2), 66–82.

Mastalerz, M., He, L., Melnichenko, Y. B., and Rupp, J. A. (2012). Porosity of coal and shale: insights from gas adsorption and SANS/USANS techniques. *Energy Fuel* 26 (8), 5109–5120. doi:10.1021/ef300735t

Melnichenko, Y. B., He, L., Sakurovs, R., Kholodenko, A. L., Blach, T., Mastalerz, M., et al. (2012). Accessibility of pores in coal to methane and carbon dioxide. *Fuel* 91 (1), 200–208. doi:10.1016/j.fuel.2011.06.026

Mendhe, V. A., Bannerjee, M., Varma, A. K., Kamble, A. D., Mishra, S., and Singh, B. D. (2017). Fractal and pore dispositions of coal seams with significance to coalbed methane plays of East Bokaro, Jharkhand, India. *J. Nat. Gas. Sci. Eng.* 38, 412–433. doi:10.1016/j.jngse.2016.12.020

Meng, Q., Xiao, Y., Shi, J., Zhao, H., Liu, Y., Wang, Y., et al. (2023). Genesis and source of natural gas in well mitan-1 of ordovician Majiagou Formation, middle-eastern Ordos Basin, China. *J. Nat. Gas Geoscience* 9, 39–51. doi:10.1016/j.jnggs.2023.12.001

Menke, H. P., Bijeljic, B., and Blunt, M. J. (2017). Dynamic reservoir-condition microtomography of reactive transport in complex carbonates: effect of initial pore structure and initial brine pH. *Acta* 204, 267–285. doi:10.1016/j.gca.2017.01.053

Norbisrath, J. H., Weger, R. J., and Eberli, G. P. (2016). Complex resistivity spectra and pore geometry for predictions of reservoir properties in carbonate rocks. *J. Petrol. Sci. Eng.* 151, 455–467. doi:10.1016/j.petrol.2016.12.033

Oyewole, E., Saneifar, M., and Heidari, Z. (2016). Multiscale characterization of pore structure in carbonate formations: application to the scurry area canyon reef operators committee unit. *Interpretation* 4 (2), SF165–SF177. doi:10.1190/int-2015-0123.1

Pan, J., Wang, K., Hou, Q., Niu, Q., Wang, H., and Ji, Z. (2016). Micro-pores and fractures of coals analysed by field emission scanning electron microscopy and fractal theory. *Fuel* 164, 277–285. doi:10.1016/j.fuel.2015.10.011

Piechaczek, M., and Pusz, S. (2015). Evaluation of the possibilities of applying fractal analysis for the characterization of molecular arrangement of carbon deposits in comparison to conventional instrumental methods. *Int. J. Coal Geol.* 139, 40–48. doi:10.1016/j.coal.2014.06.026

Qi, C., Liu, Y., Dong, F., Liu, X., Yang, X., Shen, Y., et al. (2020). Study on heterogeneity of pore throats at different scales and its influence on seepage capacity in different types of tight carbonate R-eservoirs. *Geofluids* 2020 (1), 1–7. doi:10.1155/2020/6657660

Qu, T., Huang, Z., Chen, J., Li, T., Dong, J., Li, Z., et al. (2022). Pore structure characteristics and their diagenetic influence: a case study of paleogene sandstones from the pinghu and huagang formations in the xihu depression, east China sea basin. *Math. Geosci.* 54 (8), 1371–1412. doi:10.1007/s11004-022-10022-0

Shao, X., Pang, X., Li, H., and Zhang, X. (2017). Fractal analysis of pore network in tight gas sandstones using NMR method: a case study from the ordos basin, China. *Energy and Fuel* 31 (10), 10358–10368. doi:10.1021/acs.energyfuels.7b01007

Sok, R. M., Knackstedt, M. A., Varslot, T., Ghous, A., Latham, S., and Sheppard, A. P. (2010). Pore scale characterization of carbonates at multiple scales: integration of Micro-CT, BSEM, and FIBSEM. *Petrophysics-The SPWLA J. Form. Eval. Reserv. Descr.* 51 (06).

Tan, Q., Kang, Y., You, L., Xu, F., and Meng, S. (2020). A comprehensive insight into the multiscale pore structure characterization of saline-lacustrine tight carbonate reservoir. *J. Petroleum Sci. Eng.* 187, 106744. doi:10.1016/j.petrol.2019.106744

Tu, J., Dong, Y., Zhang, B., Nan, H., Li, C., Wang, X., et al. (2016). Discovery of effective scale source rocks of the Ordovician Majiagou Fm in the Ordos Basin and its geological significance. *Nat. Gas. Ind. B* 3 (4), 330–338. doi:10.1016/j.ngib.2016.12.009

Wang, B., Tan, X., Su, W., Yan, W., Xiao, D., Guo, M., et al. (2022). Genesis and pore evolution of dolomite reservoir in the Majiagou Formation, Ordos Basin, China. *Energy Explor. Exploitation* 40 (1), 155–173. doi:10.1177/01445987211049302

Wang, J., Gao, C. L., Bai, L., Xiang, B., Liu, J., Xian, B., et al. (2023). Diagenesis and pore evolution of Cretaceous Qingshuihe Formation reservoir in western section of southern margin of Junggar Basin. *Petroleum Geol. Exp.* 45 (4), 632–645. doi:10.11781/sysydz202304632

Wang, L., He, Y., Peng, X., Deng, H., Liu, Y., and Xu, W. (2020). Pore structure characteristics of an ultradeep carbonate gas reservoir and their effects on gas storage and percolation capacities in the Deng IV member, Gaoshiti-Moxi Area, Sichuan Basin, SW China. *Mar. Petroleum Geol.* 111, 44–65. doi:10.1016/j.marpetgeo.2019.08.012

Washburn, E. W. (1921). "The dynamics of capillary flow," Physical Review A: atomic. *Mol. Opt. Phys.* 17 (3), 273–283. doi:10.1103/physrev.17.273

Wei, X., Chen, H., Zhang, D., Dai, R., Guo, Y., Chen, J., et al. (2017). Gas exploration potential of tight carbonate reservoirs: a case study of Ordovician Majiagou Formation in the eastern Yi-Shan slope, Ordos Basin, NW China. *Petroleum Explor. Dev.* 44 (3), 347–357. doi:10.1016/s1876-3804(17)30041-1

Wu, D., Zhou, J., Junfeng, R., Li, W., Wei, L., and Yu, Z. (2023). Reconstruction of depositional environment and source-reservoir confiuration relationship of ordovician Majiagou Formation in Ordos Basin, 48(2):553–567.

Wu, J., Fan, T., Gomez-Rivas, E., Gao, Z., Yao, S., Li, W., et al. (2019). Impact of pore structure and fractal characteristics on the sealing capacity of Ordovician carbonate cap rock in the Tarim Basin, China. *Mar. Petroleum Geol.* 102, 557–579. doi:10.1016/j.marpetgeo.2019.01.014

Xiong, Y., Tan, X., Dong, G., Wang, L., Ji, H., Liu, Y., et al. (2020). Diagenetic differentiation in the ordovician Majiagou Formation, Ordos Basin, China: facies, geochemical and reservoir heterogeneity constraints. *J. Petroleum Sci. Eng.* 191, 107179. doi:10.1016/j.petrol.2020.107179

Yang, L. I., Zhijiang, K. A. N. G., Zhaojie, X. U. E., and Zheng, S. (2018). Theories and practices of carbonate reservoirs development in China. *Petroleum Explor. Dev.* 45 (4), 712–722. doi:10.1016/s1876-3804(18)30074-0

Yang, Z., Liu, X., Han, X., Zhou, H., Zhan, S., Gui, X., et al. (2022). Multiple-stage injection of deep hydrothermal fluids in the dolostone reservoirs of ordovician Majiagou Formation, southern Ordos Basin. *Front. Earth Sci.* 10, 954192. doi:10.3389/feart.2022.954192

Yu, Z, Sun, L., Wu, X., Wu, D., Yao, X., Ding, Z., et al. (2012). Charactersitics and controlling factors of the middle array of Ordovician Majiagou reservoirs to the west of Jingbian gas field, Ordos Basin. *Mar. Orig. Pet. Geol.* 17 (4), 49–56.

Zhang, K., Pang, X., Zhao, Z., Shao, X., Zhang, X., Li, W., et al. (2018). Pore structure and fractal analysis of Lower Carboniferous carbonate reservoirs in the Marsel area, Chu-Sarysu basin. *Mar. Petroleum Geol.* 93, 451–467. doi:10.1016/j.marpetgeo.2018.03.027

Zhang, Q., Zhu, X. M., Chen, X., Zhu, S. F., Ji, H. C., and Jiang, Y. F. (2010). Distribution of diagenetic facies and prediction of highquality reservoirs in the lower cretaceous of the Tanzhuang sag, the southern north China basin. *Oil Gas Geol.* 31 (4), 472–481.

Zhang, Y., Yang, S., Zhang, Z., Li, Q., Deng, H., Chen, J., et al. (2022). Multiscale pore structure characterization of an ultra-deep carbonate gas reservoir. *J. Petroleum Sci. Eng.* 208, 109751. doi:10.1016/j.petrol.2021.109751

Zhao, W., Shen, A., Hu, S., Zhang, B., Pan, W., Zhou, J., et al. (2012). Geological conditions and distributional features of large-scale carbonate reservoirs onshore China. *Petroleum Explor. Dev.* 39 (1), 1–14. doi:10.1016/s1876-3804(12)60010-x

Zou, C. N., Tao, S. Z., Hui, Z., Zhang, X. X., He, D. B., Zhou, C. M., et al. (2008). Genesis, classification, and evaluation method of diagenetic facies. *Petroleum Explor. Dev.* 35 (5), 526–540. doi:10.1016/s1876-3804(09)60086-0